Coronal hard X-ray and γ-ray sources

S. Krucker
Space Sciences Lab, UC Berkeley

M. Battaglia, P. Cargill, L. Fletcher, H. Hudson, T. Kosugi, A. MacKinnon, S. Masuda, L. Sui, M. Tomczak, A. Veronig, L. Vlahos, & S. White
Various august institutions

Abstract. The solar corona supports many forms of activity that in the past have been best observed at radio wavelengths. Over the years, however, many observations of hard X-ray and γ-ray emission have also been reported. Most of these observations have not had the benefit of imaging, so that in many cases they have provided limited physical information. Now RHESSI[1] has given us a systematic view of coronal sources that combines high spatial and spectral resolution. This paper surveys the RHESSI observations in the context of prior knowledge, emphasizing new phenomena observed in the corona not directly associated with the impulsive phase. Despite the low density and hence low bremsstrahlung efficiency of the corona, we now detect coronal hard X-ray emission from sources in all phases of solar flares.

Keywords: Corona, flares, particle acceleration, X-rays

[1] The Reuven Ramaty High-Energy Solar Spectroscopic Imager; see Lin et al. (2002)

Table of Contents

1. Introduction

Energetic electrons, accelerated outside the thermal background distribution, underpin a wide variety of coronal radio sources. One might expect that these "tail population" electrons would also emit detectable levels of hard X-radiation via bremsstrahlung, which would indeed provide a more direct and less model-dependent means of characterizing them. However the hard X-ray/soft γ-ray energy range of a few keV to 10 MeV presents major challenges for sensitive instrumentation. In particular focusing optics become difficult, so that all information to date has come from the relatively high-background imaging techniques based upon image modulation (e.g., Prince et al., 1988). The RHESSI spacecraft, launched in February 2002, is now nevertheless providing a much superior observational view of this difficult domain. In this paper we describe several new types of coronal hard X-ray emission that arguably require non-thermal distribution functions accelerated away from the background Maxwellian plasma.

Thus far the coronal hard X-ray observations have been published essentially event-by-event, although Cliver et al. (1986) and Bai and Sturrock (1989) have reviewed late-phase "extended events" (for the prototype, see Figure 1). Kiplinger (1995) later showed these to be related to the production of "solar cosmic rays" (SEPs, solar energetic particles appearing in the heliosphere). These results were based mainly upon non-imaging observations; since this era we have had four hard X-ray imaging experiments (on the Solar Maximum Mission, *Hinotori*, *Yohkoh*, and now the RHESSI spacecraft, the only source of hard X-ray and γ-ray imaging for the foreseeable future). These data have allowed us to go beyond the primitive observational technique of limb occultation, and to begin to observe hard X-rays against the disk of the Sun as is common at soft X-ray, EUV, and radio wavelengths. The limb-occultation technique, however, led to our first empirical knowledge of coronal hard X-ray emission, and the stereoscopic comparison of simultaneous data with heliospheric spacecraft such as *Ulysses* and Pioneer Venus Orbiter led to the early recognition of compact footpoint hard X-ray sources as a characteristic of the impulsive phase (Hoyng et al., 1976; Kane et al., 1979).

The *Yohkoh* hard X-ray imaging observations gave us the discovery of the celebrated Masuda et al. (1994) "above-the-loop-top" source, an unexpected coronal structure appearing in the impulsive phase of a flare just at the limb. The coronal source was apparently not directly connected with the soft X-ray magnetic loops that characterize soft X-ray images of solar flares. The RHESSI data do not show such an extreme version of this type, but do reveal many other examples of

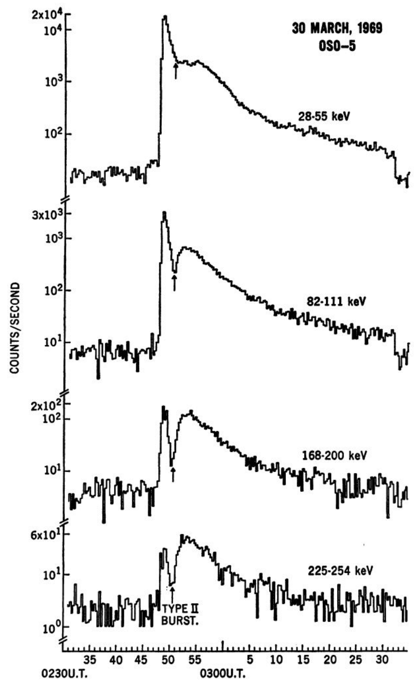

Figure 1. The "original" coronal hard X-ray event, that of March 30, 1969 (Frost and Dennis, 1971 as observed by OSO-5. This enormously energetic event came from an active region behind the limb and produced spectacular radio observations as well (e.g., Palmer and Smerd, 1972). The hard X-ray spectrum was extremely flat, approaching a spectral index $\gamma \sim 2$.

coronal hard X-ray sources as reviewed in these notes. These include what appear to be fundamentally new classes of events, notably hard X-rays appearing prior to the impulsive phase as in the γ-ray flare event of 2002 July 23 (Lin, 2002). We discuss these different types of events, as summarized in Table I, in approximately chronological order; roughly the latter half of the table consists of original RHESSI discoveries. The listing includes the so-called "superhot" sources discovered by Lin et al. (1981) for completeness even though they are apparently thermal in nature; the RHESSI data are now revealing a wide variety of intermediate cases because of its unique access to the 3-12 keV band. We also summarize the basic physics of coronal hard X-ray emission in Section 2. Although it is certainly premature to classify the small number of events that have been reported, several morphologies appear and it is likely that different physics is involved in different events. Our classifications are probably not all mutually exclusive, nor comprehensive. The radio data guarantee that other (albeit faint) sources must

Table I. Prototypical coronal hard X-ray sources

Description	Prototype event	Reference
Late phase, hard spectrum	30 March 1969	Frost and Dennis (1971)
Late phase “superhot” spectrum	21 June 1981	Lin et al. 1981
Impulsive phase “above the loop top”	13 January 1991	Masuda et al. 1994
Fast hard X-ray ejection	18 April 2001	Hudson et al. (2001)
Early-phase hard spectrum	23 July 2002	Lin et al., 2003
Coronal thick-target source	14 April 2002	Veronig & Brown 2004
Early-phase “superhot” spectrum	3 November 2003	Sui et al., in prep?
Coronal γ-ray emission	20 January 2005	Krucker et al., in prep

occur, and in Section 5.2 we discuss one of the likeliest possibilities: the direct hard X-ray detection of electrons responsible for type III radio bursts

2. Basic physics

Coronal emission in hard X-rays results from the bremsstrahlung emission of weakly relativistic (> 10 keV) electrons on ambient coronal plasma. More exotic mechanisms are possible but not likely; this subject has not been discussed recently in the literature so we present a brief discussion in Appendix A.

We do not have much detailed information about the distribution functions of the particles, nor of the physical state of the plasma in the corona, especially during disturbed conditions. The coronal hard X-ray sources discussed in this paper include (for completeness) those probably only representing the tail of essentially thermal distributions. These “superhot” sources (Lin et al., 1981) presumably represent strongly heated plasmas in which one may expect distortions from a thermal velocity distribution. The RHESSI observations, with good spectral and spatial resolution, may help in understanding these distortions, which may be represented in the coronal hard X-ray sources listed in Table I.

For ordinary flare hard X-ray sources one makes the “thick target” assumption in which the electrons actually stop (Brown, 1971a; Hudson, 1972) while radiating. This simplifies the discussion by removing the ambient density as an explicit physical parameter. For coronal sources instead we must think of ordinary thin-target bremsstrahlung.

In Appendix B we present simple formulas convenient for representing the physical parameters of these coronal hard X-ray sources. The lack of hard X-ray imaging observations in the past has meant that the spatial structures were not well understood in the past, but with *Yohkoh* and especially RHESSI we are obtaining some information now about source locations, sizes, and motions. In general the radiating electrons move in the coronal magnetic field. In static situations we could assume particle trapping describable by adiabatic motions (gyration and bounce; generally the solar field does not have the symmetry required for the third invariant). Unfortunately the coronal magnetic field is not at all static at the times of interest. Standard scenarios envisioned for eruptive flares involve a drastic restructuring of these loops, and the presence of solar energetic particles (SEPs) in interplanetary space may mean that some of these same electrons may actually escape from their coronal traps (Kontar & Krucker, in preparation). Hard X-ray source motions could correspond to plasmoids or expanding loops, and stationary hard X-ray sources to particles trapped in structures left behind in an eruption. The stable trapping of electrons is also problematic because of the possibility of loss-cone instabilities, as discussed below in Section 7.1.

In dealing with coronal hard X-ray sources, we must be alert to the distinction between trapped particles and an ordinary thermal plasma. In the latter we would expect a core Maxwellian distribution, and the normal theoretical assumption for coronal studies is that $T_e = T_i$ as well. If there are large enough populations of high-energy electrons to produce detectable bremsstrahlung, despite its inefficiency, we must also consider particle distribution functions far from a relaxed state.

3. Observations

3.1. Early-phase sources

The RHESSI observations have revealed what appears to be a new class (or classes) of coronal hard X-ray emission, namely sources that *precede* the impulsive phase. The prototype of this class are the event of 23 July 2002 (Lin et al., 2003b; Asai et al., 2004; Asai et al., 2006, Asai et al. 2007) and the limb flare on 24 August 2002, as illustrated in Figure 2. Lin et al. (2003b) pointed out that the hard X-ray spectrum in this phase of the event appears almost continuous to low energies (<10 keV), but with the characteristic Fe emission feature at 6.7 keV establishing that some background thermal plasma exists in the source. While time evolution of the thermal component is gradual, the emission at higher energies shows time variations of tens of second duration suggesting that the two components are produced by different emission mechanisms. X-ray spectral fitting reveal a relatively soft spectra that can be either represented with a power law (with power law indices around 5), or by a multi-thermal fit with temperatures up to 100 MK. However, microwaves observations. Asai et al (2007) suggest that non-thermal electrons are producing the HXR emission as well. Comparing hard X-ray and microwave observations of the July 23, 2002 event, Asai et al. (2004) found that the a single population of non-thermal electrons can produce both emissions, although rather strong coronal magnetic field strengths around 200 G are needed to match the intensities seen in HXR and microwaves.

We speculate that Yohkoh/HXT did not observe such events readily because of its “flare mode” operation, in which hard X-ray spectra were not telemetered until the hard X-ray flux reached a given threshold, which usually corresponded to the onset of the main impulsive phase. Thus an interesting source prior to the impulsive phase would systematically not have been properly observed (but see Fárník et al., 2003, for an early-phase observation resulting from an unprogrammed mode change).

3.2. Gradual late-phase sources

The event of 30 March 1969 (Frost and Dennis, 1971) occurred in an active region known circumstantially to have been some distance behind the solar limb (Smerd & Weiss, 1971), so that the hard X-rays visible from the Earth-orbiting OSO-5 spacecraft probably originated from relatively high in the corona. Two other examples of quite similar events were reported with OSO-7 data (Hudson, 1978; Hudson et al., 1982); such events are characterized by flat hard X-ray spectra (power-law index $\gamma \sim 2$), gradual time profiles, low microwave peak frequencies, anomalously weak soft X-ray emission, and association with coronal radio bursts. RHESSI has now observed sources in this category (see below) but the ten years of *Yohkoh* did not produce a clear example from HXT[1]; we attribute this to the rarity of prototypical events and to the low dynamic range of modulation-based imaging instruments.

Nevertheless a related pattern appears in the so-called “soft-hard-harder” spectral evolution of many long-duration hard X-ray events (Cliver et al., 1986; Kiplinger, 1995). This spectral pattern differs from the otherwise ubiquitous “soft-hard-soft” pattern associated with the impulsive phase (Parks and Winckler, 1969; Hudson and Fárník, 2002; Grigis and Benz, 2004). From a non-imaging perspective, the hard

[1] Yohkoh’s Hard X-ray Telescope; see Kosugi et al., 1992)

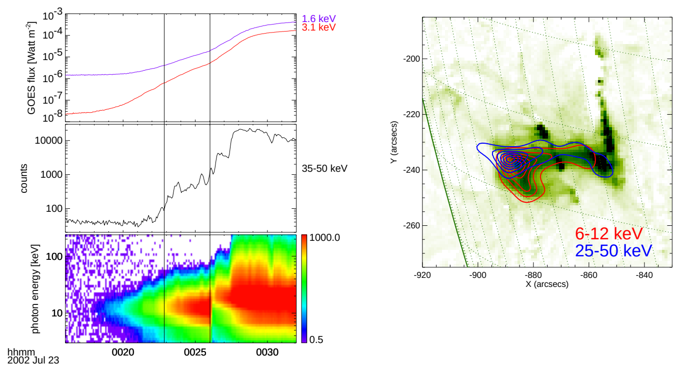

Figure 2. Example of coronal emission before the impulsive phase in the July 23, 2002 flare. (left) X-ray time profiles and spectrogram from GOES and RHESSI showing thermal emission with a gradual evolution and a second component at higher energy with fast time variations of tens of seconds. (right) Imaging reveals that the fast time variation component mostly comes from the corona. RHESSI contours in the thermal range (red) and at higher energies (blue) are shown for the time range outlined by vertical bars in the figure to the left. The shown image is a TRACE 195Åimage taken at 00:26:00 UT.

X-ray spectrum of such a source consists of a gradual, continuously hardening component plus a serie.s of spikes with soft-hard-soft evolution. Often these spikes become more gradual as the event develops, as illustrated in Figure 4 (and as seen in the earliest, non-imaging observations, from the TD-1A spacecraft; see Hoyng et al., 1976).

The RHESSI imaging observations have added a new feature for the interpretation of these late-phase sources. Because of their long duration, a thin-target explanation might be imagined, such that the hard X-ray emission would come predominantly from the corona. However it now appears (Krucker. in preparation 2007) that these late sources emit hard X-radiation mainly from footpoints, as with ordinary flare loops. Figure 5 illustrates this for one of the flares of January 2005. The footpoint nature of these late-phase events had already been pointed out by (Qiu et al., 2004).

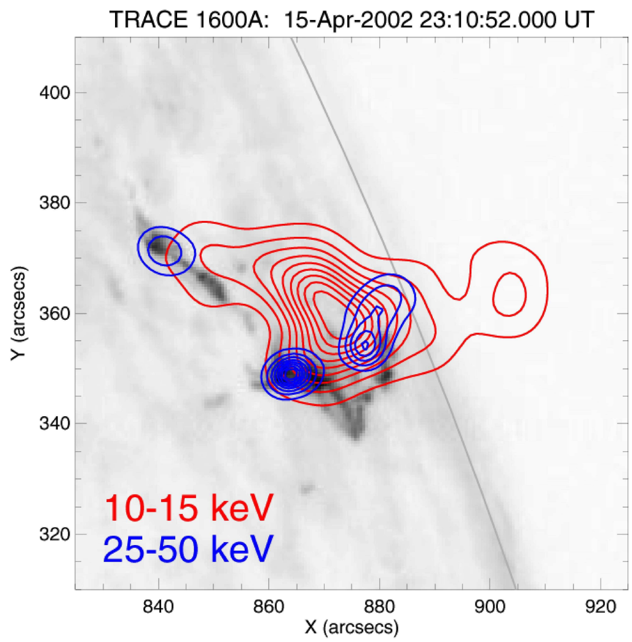

Figure 3. Coronal X-ray source above a flare of 2002 April 15, a feature interpreted by Sui & Holman (2004) as the coronal end of a reconnecting current sheet prior to its explosive eruption.

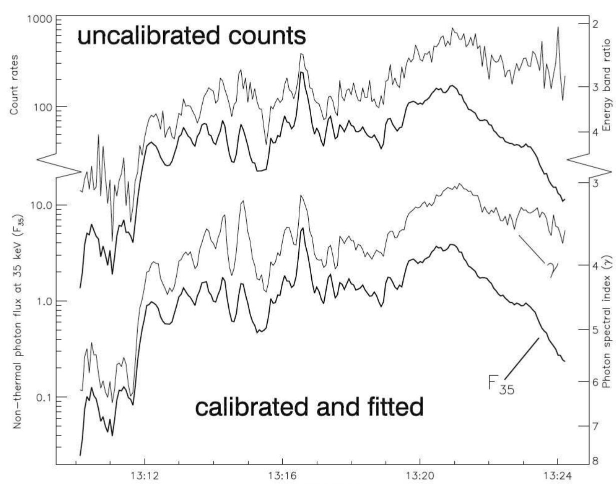

Figure 4. RHESSI non-imaging hard X-ray observations of an extended hard X-ray event, as analyzed by Grigis and Benz (2004), showing the joint variation of spectral flux at 35 keV and spectral index γ. Note the steady evolution from spiky bursts exhibiting soft-hard-soft morphology, upon which a more gradual hardening component can be discerned.

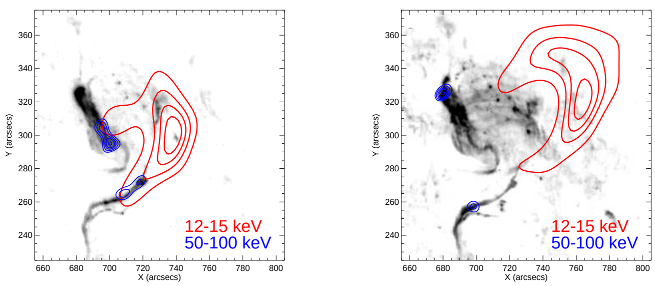

Figure 5. Footpoint sources in the late phase of one of the January 2005 flares.

3.3. The impulsive phase

3.3.1. *The Masuda flare and the view from Yohkoh*

The *Yohkoh* observations of what is now universally termed the "Masuda flare" Masuda et al. (1994) showed the presence of high-energy electrons in the corona during the impulsive phase; it is possible that the pioneering stereoscopic observations of Kane et al. (1979) spotted a similar phenomenon. *Yohkoh* directly imaged the hard X-rays from the 13 January 1992 Masuda flare, revealing it to lie above the loop tops of what appeared to be a classical loop flare with bright footpoints. This source occurred during the impulsive phase of the flare, in a region of low density (i.e., with no bright soft X-ray emission nor apparent magnetic connection to the footpoints), so it immediately raised questions about the bremsstrahlung efficiency (Wheatland and Melrose, 1995a; Hudson and Ryan, 1995; Fletcher and Martens, 1998). At the same time the morphology matched the cusp geometry commonly taken to imply the presence of an essentially vertical current sheet above the flaring loops. The evident presence of non-thermal particles in this geometry then led to much discussion of the classical large-scale magnetic reconnection models of solar flares, as pointed out by Masuda et al. (1994).

The Masuda observation proved difficult to reproduce, but extensive further analysis of the original 1992 flare continued (e.g., Alexander and Metcalf, 2002; Aschwanden et al., 1999; Metcalf and Alexander, 1999; Petrosian et al., 2002). The novel features of the original Masuda flare were its location *above* the soft X-ray looptop during the impulsive phase, and a non-thermal spectral signature. There is some confusion in the literature between this source and the more common thermal loop-top sources, which have their own interesting properties. This confusion has been amplified by the unusual characteristics of these ordinary loop-top sources; they generally have a bright soft X-ray feature at the apparent loop top (Acton et al., 1992), which can might be interpreted as an anomalous overpressure because the soft X-ray emissivity typically increases monotonically with pressure, ie as a function of the product nT (Kahler, 1976). However any such overpressure should drive flows that eliminate it promptly. Alternatively, the loop-top brightening might be evidence of line-of-sight effects in a cusp structure, which however would suggest a high plasma beta.

The paper originally citing the Masuda flare (Masuda et al., 1994) has been cited many hundreds of times, and has had an enormous influence on the development of flare theory. Although it was a single event, and almost unique, its detailed analysis therefore has seemed important. The following list describes its observational properties Masuda et al. (1994), with some guesses from possibly related events (Masuda thesis; Shibata et al. 1995). We annotate this list with letters indicating an item's relevance to the following questions: (a) Does energy release take place above the looptop? (b) Is it related to large-scale magnetic reconnection (e.g., Figure 6? (c) Is the source nonthermal? (d) Is it thermal? (e) Is it from the footpoint electron population? For each question, an upper-case letter indicates affirmative and a lower-case letter negative.

1. The source is located high above the corresponding soft X-ray loop. ABcD
2. It is located in a high-temperature (>20MK) region defined by a two-filter soft X-ray temperature map. AD
3. Its time profile is similar to that of the footpoint sources, but at low time resolution. AE
4. It is clearly seen in the *Yohkoh*/HXT M2-band (33-53 keV), and sometimes in the H-band (53-93 keV). C
5. Its spectrum is relatively hard, but slightly softer than that of the footpoint sources. CD
6. The size of the source is compact. cd
7. At higher energies, the source is located at higher altitudes. D
8. The soft X-ray loop may show a cusp-like structure. B

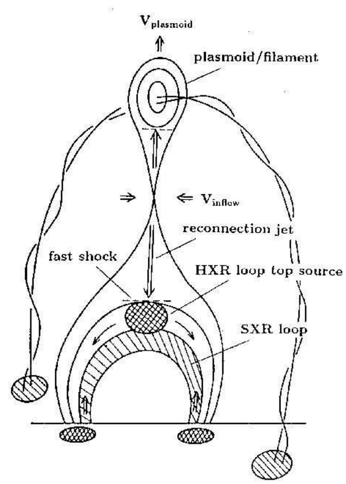

Figure 6. The Shibata version of the standard reconnection cartoon.

9. A super-hot (30-50 MK) thermal HXR source is located below the source. B

10. In an event which has a larger discrepancy between the HXR source and the SXR looptop source, a faster SXR plasmoid ejection is observed, and also the speed of the SXR loop evolution (increase in height) is faster. B

A further characteristic of the loop-top sources is the clear existence of a gradient in temperature towards greater heights in a flare loop system. Such a gradient is naturally explained by the standard 2D reconnection model, in the sense that newly-reconnected loops appear always at greater heights, and since there has been no time for evaporation to occur and establish a quasi-static equilibrium loop structure, the plasma temperature should be at least instantaneously higher at the loop tops. Such an effect is often dramatically evident in the TRACE 195Å images. This channel has a spectral passband with two maxima, one showing hotter loops (Fe XXI response) at higher altitudes, and the other showing loops after cooling to ordinary coronal temperatures (the nominal Fe XI, XII passband; see, e.g., Warren et al., 1999). The higher temperatures of the loop-top sources must also, to a certain extent, reveal the longer conductive cooling times of longer loops: $\tau_{cool} \propto \ell^2$.

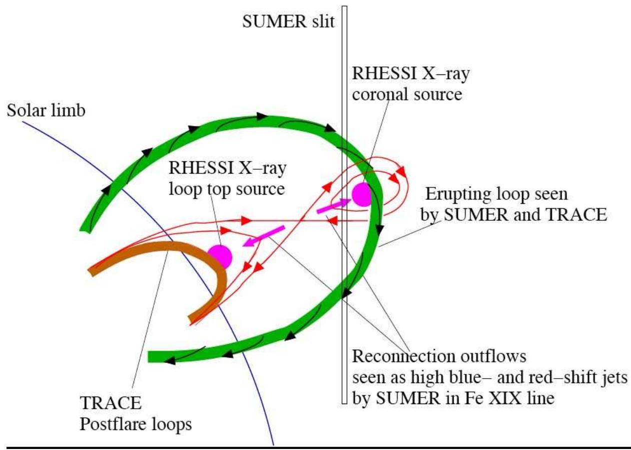

Figure 7. Sketch of the multiwavelength observations of Wang et al. (preprint, 2007) showing an event of April 16, 2002 well-observed spectroscopically by SUMER and in RHESSI X-ray images.

3.3.2. *SUMER/TRACE/RHESSI observations*

In a remarkably well-observed limb flare of April 16, 2002 there were simultaneous observations from RHESSI, TRACE, and SOHO, the latter most interestingly including SUMER observations with high-resolution UV spectroscopy from a slit positioned in the corona above the flare (Goff et al., 2005a; Wang et al. 2007 preprint). The spectroscopy revealed the presence of concentrated hot (Fe XIX) flows at the altitude of the SUMER slit, some 40 Mm above the flare. These flows, both blue and red shifts in the "correct" relationship for the standard model, had speeds consistent with a reasonable value for the Alfvén speed. These flows also matched the position and motion of the coronal X-ray ejecta observed by RHESSI. Figure 7 shows the relationships of the various observations.

3.4. Coronal gamma-ray sources

RHESSI provides for the first time imaging above 100 keV and in the γ-ray range (e.g., Figure 8. This allows us to image high-energy sources in flares that were before only seen in spectral observations. Nevertheless, the observations are limited by counting statistics and dynamic range, and we can produce images in the γ-ray range only for the largest flares with best counting statistics. The three RHESSI flares with best counting statistics in the γ-ray range all show non-thermal electron bremsstrahlung emission from their footpoints but all also have coronal γ-ray sources (Krucker et al. 2007). The coronal

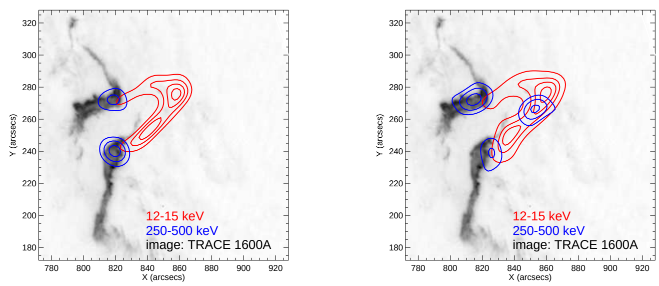

Figure 8. Imaging of January 20, 2005 flare during the γ-ray peak (left, 06:43:32-06:46:40UT), and during the decay of the emission (right, 06:46:44-06:55:01UT). Both figures show a TRACE 1600Å images taken at 06:45:11UT overplotted with 12-15 keV (red) and 250-500 keV (blue) contours. The 12-15 keV image is reconstructed using a MEM algorithm and the shown contour levels are 30, 50, 70, 90%, while the CLEAN algorithm is used for the reconstruction of 250-500 keV images and 50, 70, 90% contours are displayed. During the peak the γ-ray emission is coming from footpoints, while later an additional coronal source is visible.

sources are most prominent during the exponential decay of the γ-ray emission and show an extremely hard spectrum with a power law slope between $\sim$1.5 and $\sim$2. The parameters of the coronal sources are similar to the partly occulted flare recorded March 30, 1969 (Frost and Dennis, 1971) that also showed coronal exponentially decaying emissions with similar intensity and also a very hard spectrum ($\gamma \sim$2). The observed spectral index of the coronal source in the 200-800 keV range is close to the hardest theoretically possible bremsstrahlung spectrum, suggesting that the emission is produced by electrons at even higher energies (>1 MeV). These observations directly imply that flare-accelerated high energy electrons ($\sim$MeV) reside long enough in the corona and lose their energy by collisions producing γ-ray emission, while lower-energy electrons precipitate to the footpoints without losing significant energy in the corona. Hence, the energy dependence of the trapping time should be steeper than for the collisional loss time and roughly equal around $\sim$1 MeV. The theoretical situation is unclear but the new data should help substantially.

3.5. Hard X-ray emission from the high corona

As discussed above, the partial occultation of a solar flare by the solar limb is an excellent tool for studying faint coronal HXR emissions without competition from the very bright emissions of the footpoint sources. For flares occurring 20 or more degrees behind the solar limb, not only the HXR footpoints but also the main thermal and non-thermal HXR emissions from the corona are occulted, and flare-related emissions from the high corona (>200? Mm above flare site) can be seen. Kane et al. (1979) [Is this the right reference? - HH] reported HXR emissions from a flare occulted by 40 degrees as seen from Earth (see Figure 9. Despite this large occultation height, roughly a third of a solar radius, HXR emissions were observed up to 80 keV, with a rather hard spectrum ($\gamma < 3.5$). Other high coronal events were observed by *Yohkoh* Hudson et al. (2001) as well as RHESSI Krucker and Lin (2007) revealing that high coronal emission related to flares are common. In particular, Krucker and Lin, 2007 showed that all fast (v¿ 1500 km s-1) backside CMEs that originated from flares occulted by 20 to 45 degrees show related HXR emissions from the high corona. Multi-spacecraft observations Kane et al., Krucker and Lin (1979, 2007) reveal that the HXR emissions from the high corona occur during the impulsive phase of the flare simultaneously with the HXR footpoint emissions. The reported time profiles all look similar and show a relatively simple time evolution, with a fast rise and a slower exponential decay. The exponential decay is surprisingly constant, lasting sometimes several minutes without significant deviation, and the photon spectrum exhibits progressive spectral hardening. This might indicate that mostly collisional losses – without further acceleration – dominate. Density estimates of the ambient plasma supports this, as the estimated collisional loss times of 25 keV electrons have comparable time scales. The total energy content of the non-thermal electrons in the high corona in such cases is estimated at about 0.1 of the total flare energy Krucker and Lin (2007).

Yohkoh observations revealed that the HXR emissions from the high corona may move upward with a velocities of around 1000 km s^{-1} in the same direction as the as the CME (Hudson et al., 2001). Recent imaging observations by RHESSI Krucker and Lin (2007) also show upwards motions, with similar velocities, but additionally reveal that the high coronal sources may be large (>200$''$) and expand in time with velocities of $\sim$400 km s^{-1}. The total energy content of non-thermal electrons in high corona is estimated to be 0.1. of the total flare energy. However, the relative number of energetic electrons in the high corona can be of the same order of magnitude as the number

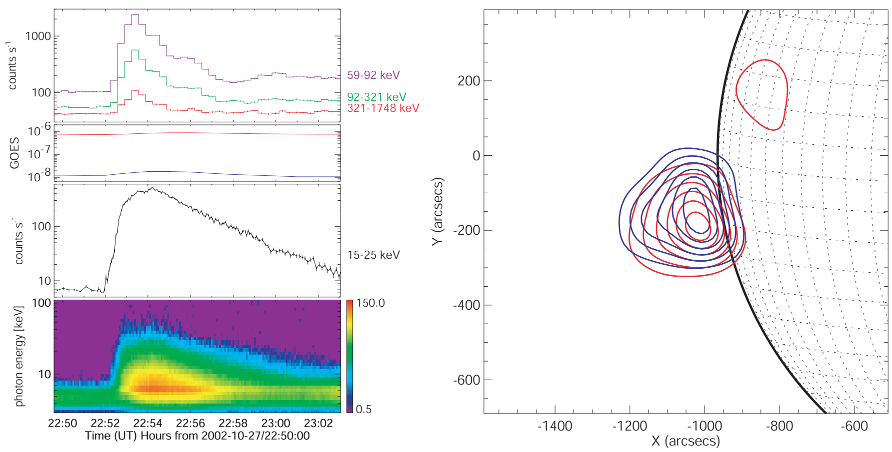

Figure 9. (left) Time profile of the October 27, 2002 event. This was seen on-disk from Mars, but for Earth-orbiting spacecraft the flare site was occulted by at least 200 arcsec (0.2 $R_{\odot}$). From top to bottom the panels show: (1) GRS X-ray and γ-ray time profiles seen from Mars (entire flare is seen), (2) GOES soft X-ray flux seen from Earth, (3) RHESSI 15-25 keV time profile seen from Earth, (4) RHESSI HXR spectrogram, (5) radiospectrogram observations from Culgoora Observatory and from (6) WIND/WAVES. (right) RHESSI X-ray imaging in the thermal range (3-7 keV, red contours) and non-thermal range (10-30 keV, blue contours) reveal large sources (>200 arcsec) seen just above the limb. The RHESSI CLEAN algorithm was used to reconstruct these images, and the contour levels shown are at 15, 30, 45, 60, 75, and 90 % of the maximum. The thermal emission on disk around (-800/200) is from AR10717 and is already present before the flare occurs.

of thermal elelctrons (Krucker & Lin 2007). This suggests that the HXR-producing electrons are within large magnetic structures related to CMEs, and may contribute to their energetics. We return to the relationship between coronal hard X-rays and CMEs in Section 5.1.

4. Statistical studies of coronal hard X-ray emissions

4.1. Pre-*Yohkoh* (non-imaging)

The case-by-case observations of coronal sources from the early non-imaging missions were reviewed by Cliver et al., 1986. This work clearly established a pattern from these scattered events, of which the prototype was the event of March 30, 1969, shown in Figure 1. The pattern specifically invoked a “soft-hard-harder” morphology of spectral evolution, something sharply distinguishable from the “soft-hard-soft” morphology of the impulsive phase. This type of temporal evolution strongly suggests particle trapping in the solar corona, with the gradual hardening resulting from the erosion of the low-energy particles because of collisional energy losses. Thus it was surprising when Kiplinger (1995) found a good correlation between such events and proton events, though to arise via shock acceleration on open field lines much further from the Sun.

4.2. *Yohkoh*

A statistical survey of partially occulted flares observed by Yohkoh reveals the existence of coronal HXR emissions besides the main thermal sources in most events (Tomczak, 2001), but the limited energy resolution of Yohkoh/HXT makes it often difficult to separate an additional component at high energy from the main thermal emission. The relative source location of the coronal HXR emission is found to be only slightly displaced (>5 arcsec) from the thermal SXR emission in all cases expect the Masuda flare (Tomczak, 2001, Petrosian et al., 2002).

[Michal has new material here that we can incorporate at ISSI perhaps – HH]

4.3. RHESSI

RHESSI observations provide for the first time good enough spectral resolution to clearly separate main thermal emissions from emissions at higher energies. Battaglia and Benz (2006) analyzed fiveRHESSI flares with coronal sources well separated from the related HXR footpoints emissions, finding also faint HXR emissions with a soft power law spectra in the corona in addition to the thermal emissions (Figure 10). Statistical results of partially occulted flares observed by RHESSI (Krucker & Lin 2007, in preparation) confirm the Yohkoh results showing in addition to thermal HXR emissions a second coronal component in at least 90% of all events (Figure 10). The second component is most prominent during the rise phase of the thermal emission, has a much softer spectrum than spectra of on-disk flares, and its centroid position is often co-spatial or within a few arcsec of the thermal emission although for a few events clear separations are observed as well. In some events, coronal thin target emission from flare-accelerated electrons that afterwards lose their energy by collisions in the chromosphere could produce this second component at least in some events (Krucker & Lin 2007, in preparation), however, for others events, a simple thin target model does not work (Battaglia and Benz (2007a)) and non-collisional losses might be important as well.

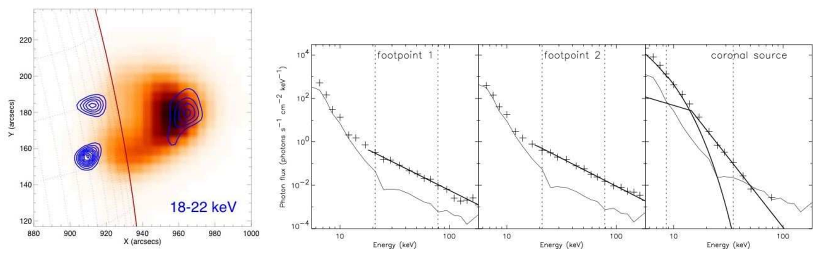

Figure 10. Imaging spectroscopy with RHESSI: The July 13, 2005 flare around 14 UT shows coronal emission spatially well separated from the HXR footpoints, making it easy to get spectra for the coronal sources and HXR footpoints separately. Left, RHESSI 18-22 keV contours averaged over the time period between 14:13:50 and 14:15:48 UT overplotted on a GOES SXI image taken at 14:17:05 UT. Right, imaging spectroscopy results from Battaglia and Benz (2006).

5. Source environments

[For the first two of the subsections here, there is not really any observational material except for circuitously indirect things. However it was my feeling that we should put these things into context. At some level the electron beams in type III bursts (ditto type II) should make HXR for some lucky instrument to see. So, what do we know about limits and what sensitivity might be required, and also what really could we learn? – HH]

5.1. Fast HXR ejecta and CMEs

[This section is just a gleam in the eye. It might be redundant observationally, or it might be brilliant conceptually; we shall see! – HH]

5.2. Type III bursts

One well-anticipated type of coronal source would be the hard X-ray counterpart of the type III radio burst, interpreted since the earliest times (e.g. Wild et al., 1963) as the outward motion of streams of non-thermal electrons, as directly confirmed in interplanetary space (e.g., Lin, 1970). Such HXR emissions would trace the motion of the electron beams in the corona and reveal their acceleration region, as well as showing how they escape into interplanetary space. Type III bursts often (33%) occur during solar flares (Benz et al., 2005), especially during the impulsive phase, but also often in the absence of major flares (Kane et al., 1974). At such times soft X-ray observations tend to show the presence of jets, invariably with a X-ray microflare (compact soft X-ray loop) near the foot of the jet (Aurass et al., 1994; Raulin et al., 1996). Sometimes, but by far not always, hard X-ray emissions and type III radio bursts are seen simultaneously (Kane, 1972, Stewart, 1978, Aschwanden et al., 1995, Arzner and Benz, 2005). However, the observed hard X-ray emission appears generally not to be thin-target emission from the escaping electrons, but thick-target emission from simultaneously accelerated downward-moving electron beams that lose their energy in the chromosphere. For some events, in-situ observations of escaping electrons are additionally available, allowing a comparison of the escaping and downwards-moving components (Daibog et al., 1981, Pan et al., 1984, Krucker et al. 2007, ApJ, submitted). The electron spectra of the downward moving and escaping electrons are found to be correlated suggesting a common acceleration, but only a small fraction (typically less than 1%) of the electrons escape into interplanetary space, while most of the accelerated electrons loss their energy by collisions in the chromosphere. Therefore, the faint thin-target emission of the few escaping electrons is very difficult to detect in the presence of the brighter thick-target emission of the much larger number of downward-moving electrons. Christe et al. (2007, submitted) report HXR emission temporally related to radio type III bursts in the absence of flares, suggesting that thin-target emission of the escaping electrons might have been observed. However a detailed analysis reveals that the observed HXR emission is not bremsstrahlung emission from escaping electrons, but rather thermal emission possibly related to the acceleration mechanism itself. Christe et al. concluded that the sensitivity and the dynamic range of RHESSI observations are not high enough to detected non-thermal HXR emission from type III burst. Assuming that the type-III-producing electron beam consists of 10^{33} electrons above 5 keV (consistent with in-situ electron measurements near 1 AU, Lin 1973), and that these electrons propagate away from the Sun beginning from a density of $5{\times}10^9\mathrm{cm}^{-3}$ (600 MHz), RHESSI would only detect about 0.5 counts per second, not enough for a clear detection (at 3 to 15 keV, the RHESSI background is at least 30 counts per second). Hard X-ray instruments with higher sensitivity, lower background, and larger dynamic range are need to detect the thin target emission from the escaping electrons routinely. This would make it possible to image the acceleration site, trace electron beams in the corona and reveal the magnetic connection between the acceleration site, the HXR footpoints, and the open field lines along which electrons escape into interplanetary space. Such emissions theoretically exist at a level not far below present limits. Focusing optics in the hard X-ray range might be able to provide the additional sensitivity needed (e.g.,Ramsey et al., 2000).

5.3. Coronal thick targets

In most flares, the observed HXR radiation is primarily from the footpoints of magnetic loops (Sakao, 1994) assumed to be due to thick target emission of fast electrons stopped in the collisionally dense chromosphere (Brown, 1971b). However, recent RHESSI observations revealed a new class of events in which the HXR emission is predominantly from the coronal flare loop, with little or no emission from the footpoints (Veronig and Brown, 2004).[2] These flares are characterized by steep nonthermal power-law X-ray spectra ($\gamma \gtrsim 6$) and high column densities ($N \gtrsim 10^{20}$ cm^{-2}) in the observed soft X-ray flare loops, which led to the interpretation that in these events the corona itself acts as a thick target to the injected electron beam, and thus most electrons never reach the chromosphere to produce HXR emission there.

Figure 11 shows RHESSI light curves in two energy bands, a RHESSI CLEAN image sequence, and a RHESSI spectrum (integrated over one of the HXR bursts) for the coronal thick-target event that occurred on 14/15 April 2002 (GOES M3.2). The 25–50 keV count rate shows rapid fluctuations with many individual peaks of typical time scales of about 30 s indicative of nonthermal processes, whereas the 6–12 keV light curve shows a smooth gradual increase indicative of thermal emission. The plotted RHESSI images were integrated over individual HXR peaks. The hard 25–50 keV images show emission primarily from within the coronal loop (most concentrated at the loop-top), as outlined in the soft 6–12 keV images, and only weak footpoint emission. The spectrum in Figure 11 demonstrates that the emission $\gtrsim$20 keV, which is predominantly coronal, is dominated by the (steep) nonthermal power-law component.

We define a stopping energy $E_{\rm loop} = \sqrt{3KN} \simeq 8.8\sqrt{N_{19}}$ [keV], where N is the coronal loop column density and $N_{19} = N/10^{19}$ [cm^{-2}]. Electrons with energies E below the stopping energy must remain in the corona (Brown, 1973). In order to stop, e.g., a 25 keV electron, a mean loop column density of $\sim$$10^{20}$ cm^{-2} is needed. Indeed, loop column densities as high as 10^{20} cm^{-2} were observed already at the beginning of the two events studied by Veronig and Brown (2004) which increased to several times 10^{20} cm^{-2} later on, sufficiently high to stop 50 keV electrons.

The enhanced coronal (column) densities observed during solar flares are generally attributed to radiatively unstable evaporation of chromospheric matter heated to $\gtrsim$$10^5$ K by electron beams or by thermal conduction (Neupert, 1968; Brown, 1973; Antiochos and Sturrock, 1978).

[2] Though we note that one such event where the HXR emission is mainly coronal was already reported from Yohkoh observations (Kosugi et al., 1994).

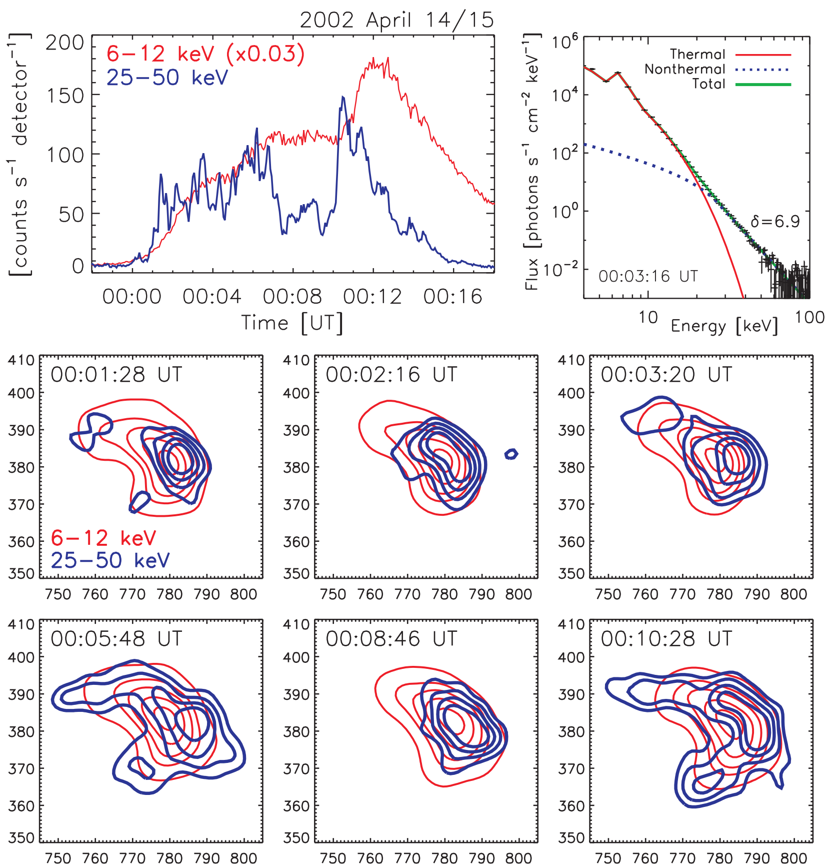

Figure 11. 14/15 April 2002 coronal thick target event: RHESSI light curves and CLEAN images in the 6–12 and 25–50 keV energy bands together with a RHESSI spectrum integrated over the burst at ∼00:03:30 UT (roughly corresponding to the third image in the sequence).

In coronal thick target events, the electron beam is very efficient in heating the coronal plasma since it deposits most of its energy there and not into the chromosphere. As a consequence, in these events the increase in column density due to chromospheric evaporation is only indirectly driven by the accelerated electrons. The beam electrons heat the corona which acts as a thick target to them, and consequently chromospheric evaporation is driven by the heat flux from the heated coronal plasma to the chromosphere, whereas in "normal" HXR events chromospheric evaporation is predominantly due to fast electrons that dump their kinetic energy into the chromosphere.

For thick-target HXR emission, the ratio R of the footpoint ($I_{\rm fp}$) to the total ($I_{\rm tot}$) emission at photon energy ϵ depends on the stopping

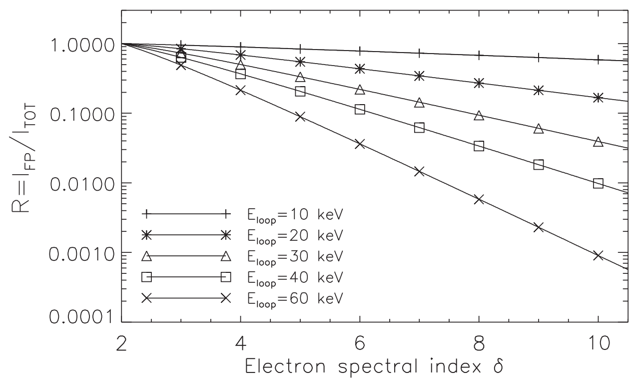

Figure 12. Ratio R of footpoint emission $I_{\rm fp}$ to total emission $I_{\rm tot}$ calculated at photon energy $\varepsilon = 25$ keV for a thick target model plotted as a function of electron beam spectral index δ for five different values of the stopping energy $E_{\rm loop}$. (From Veronig et al., 2005.)

energy in the loop, $E_{\rm loop}$, and on the electron beam spectral index, δ, namely

$$R = \frac{I_{\rm fp}(\varepsilon)}{I_{\rm tot}(\varepsilon)} = \frac{(\delta-2)}{2} B\left(\frac{1}{1+(\varepsilon/E_{\rm loop})^2}, \frac{\delta}{2}-1, \frac{1}{2}\right)\left(\frac{\varepsilon}{E_{\rm loop}}\right)^{\delta-2} \quad (1)$$

where $B(a, b, c)$ denotes the incomplete beta function (cf. Veronig and Brown, 2004) and for thick target emission $\delta = \gamma + 1$. In Figure 12 we plot this ratio at photon energy $\epsilon = 25$ keV for different values of stopping energy and beam spectral index. The figure shows that in order for a coronal thick target event to occur, two criteria have to be fulfilled: a) the stopping energy $E_{\rm loop}$ and ergo the coronal column density N has to be high, and b) the injected electron beam spectra have to be steep. On the other hand, in "normal" events with spectra $\delta \lesssim 5$ and stopping energies $E_{\rm loop} \lesssim 20$ keV (i.e., $N \lesssim 5 \cdot 10^{19}$ cm^{-2}) the footpoint emission is expected to be much stronger than the coronal one, consistent with observations.

Further examples of coronal thick-target events have been reported in addition to the 14/15 and 15 April 2002 events investigated in Veronig and Brown (2004). One of them is the homologous M-class flare that occurred on 16 April 2002, studied by Sui et al. (2004) and Goff et al. (2005b). This event is probably the most paradigmatic coronal thick-target example, since during the overall flare duration the non-thermal HXR radiation outlines the whole coronal loop, as observed in TRACE EUV images. Jiang et al. (2006) report three examples where the coronal HXR emission dominates over the footpoint emission, but only after the HXR peak. These events have nonthermal powerlaw spectra, which are interpreted as thick-target coronal emission due to the flare-increased column density. Lin et al. (2003a) speculate that in the early phase of the the 23 July 2002 X-class flare, where the HXR emission is purely coronal, the spectra showing a broken power-law hint at thick-target emission in the corona.

Why are thick-target coronal HXR sources interesting? Generally, as for any type of coronal HXR source, they contain information about the flare acceleration process as well as about the ambient coronal plasma conditions. More specifically, thick-target coronal HXR sources indicate that high densities (several times 10^{10} cm^{-3}) do obviously sometimes exist in the corona even *before* a flare. This is not straightforward to explain. Veronig et al. (2005) showed, for the 14/15 April 2002 thick-target coronal flare, that an earlier had event occurred in the same set of nested loops, and gave rise to the enhanced column densities observed. Thus, the later event occurs under different initial plasma conditions due to the dense material that filled the loop during the first flare. This new material would strongly affect the propagation of the electron beam injected during the later event (see also the SMM double flare discussed in Strong et al., 1984).

However, in our standard 2D eruptive flare model, the acceleration is assumed to occur above the loop at the instantaneously reconnecting field lines which change from an open to a closed configuration. In this scenario, the electrons accelerated in the later event, would not be injected into the previously activated loops of increased density. Thus, this interpretation only works if in the later, i.e. the thick target coronal event, the electrons are accelerated *inside* the loops which were filled with chromospheric matter during the previous event, or if one takes into account a 3D situation. Bone et al. (2007) proposed such an interpretation in terms of a sequence of magnetic reconnections between multiple loop systems in a 3D field geometry assuming that the dense loops created during the first flare became unstable (e.g., due to a high-beta disruption) leading to particle acceleration into a dense coronal environment.

Finally, we note that a thick-target coronal event can be considered as the extreme case of an intermediate thin-thick target coronal flare, as analytically modeled by Wheatland and Melrose (1995b) based on *Yohkoh* observations. These authors assumed very high coronal flare densities, of the order of 10^{12} cm^{-3}, and coronal column densities in the range $1 \cdot 10^{20} \lesssim N \lesssim 7 \cdot 10^{20}$ cm^{-2}. They derived a simple analytical model to predict the relationship between the coronal and footpoint HXR emissions in such a dense flare scenario, where the corona acts either as a thick or thin target depending on the injected electron energy. This differs from the purely thick target coronal events where in addition to the high coronal loop column densities the injected electron spectra are very steep, and thus the number of electrons falls off so steeply towards high energies that there are not sufficient electrons to reach the chromosphere and produce substantial HXR footpoint emission.

The Wheatland and Melrose (1995b) model proposes that electrons with energies below the coronal stopping energy, $E < E_{\rm loop}$, experience the corona as a thick target, whereas for electrons with higher energies, $E > E_{\rm loop}$, it acts as a thin target. The model predicts that in the coronal source the photon spectral index γ below $E_{\rm loop}$ should be equal to that in the footpoints above $E_{\rm loop}$ (thick target: $\gamma = \delta - 1$), whereas the coronal source at photon energies above $E_{\rm loop}$ should reveal a power-law spectral index γ about 2 steeper (thin target: $\gamma = \delta + 1$). These predictions have been tested by Battaglia and Benz (2007b) ...

[We should get Marina to continue this a bit – HH]

[I think we need some comments about the detectability of coronal thick targets as microwave free-free sources – HH]

6. Thermal/low-energy phenomena

6.1. "Superhot" coronal sources

This subject began with the observations of Lin et al. (1981), who used a pioneering high-resolution hard X-ray spectrometer to observe *thermal* hard X-rays, for which the effective plasma temperature exceeded that observed at lower energies by, e.g., GOES. Such "superhot" sources form a bridge between thermal and non-thermal bremsstrahlung emission, and may give us some clues to the energy conversion process. "Superhot" here means T >30 MK, close to the highest temperatures inferrable from GOES photometry (Garcia, 1994), but the hard X-ray "temperatures" can be large enough to cause confusion with the (non-thermal) power-law interpretation of the spectrum.

6.2. Parallel motions

[The material below is edited input from Linhui, but he may not like the section title. Any ideas? - HH]

Sui et al. (2006) selected a special category of RHESSI flares, called "early impulsive flares," in which plasma preheating (i.e. heating before particle acceleration) is minimal. They selected RHESSI flares in

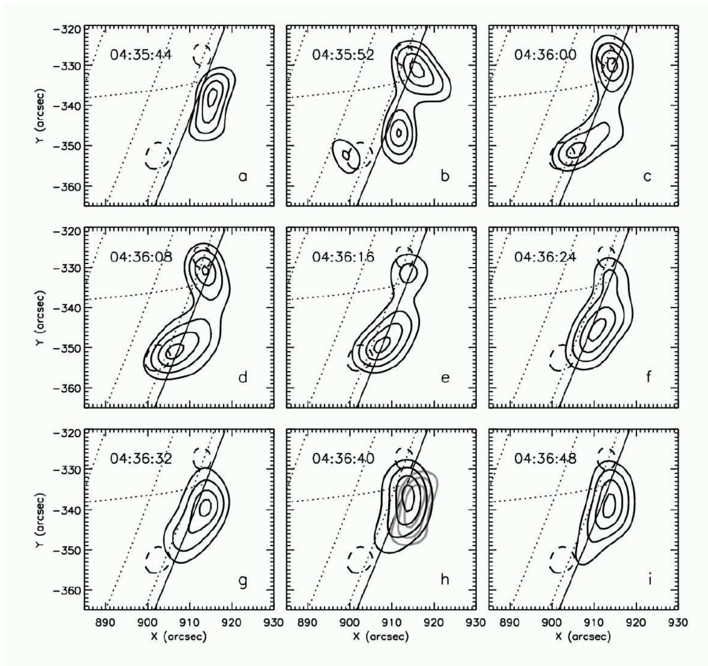

Figure 13. RHESSI 3-6 keV maps of the November 28, 2002 flare. To show the footpoint locations, the 25-50 keV contour image (dashed contours) at the hard X-ray peak time is overlaid in each panel.

which the >25 keV hard X-ray flux increase is delayed by less than 30 s after the flux increase at lower energies. By avoiding bright flare loops resulted from the preheating in typical flares, such flares allow us to detect nonthermal sources very early. This is an opportunity to obtain valuable information about the early evolution of the energetic, nonthermal electrons inside the loop.

A new type of coronal source motion, along the flare loops and apparently therefore parallel to the magnetic field, has been seen in some of these early-impulsive flares. RHESSI 3-6 keV images of a flare on November 28, 2002 are shown in Figure 13. A coronal source appears above the limb at the beginning of the flare. As the flare progressed, this source appeared to split into two separate coronal sources moving downward along the flare loop. At the time of the HXR peak, the two sources reached their lowest level, near the footpoints. After that, they moved upwards and eventually settled at the top of the loop. The downward speed was estimated at 500-700 km/s, while the upward speed was only about 340 km/s. Similar downward and upward motions can also be seen in images at other energies between 6 and 25 keV.

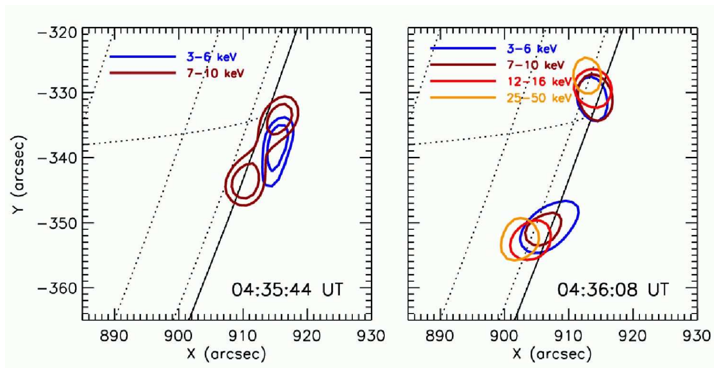

Figure 14. RHESSI images at different energies early in the November 28, 2002 flare.

During the period of the downward motion, the higher-energy sources were always located lower than the lower-energy sources (see Figure 14). Because such an energy distribution is consistent with the thick-target model, which predicts that the high-energy electrons penetrate deeper into the atmosphere before completely losing their energy (Brown et al., 2002), Sui et al. (2006) suggested that the apparent motion could be caused by the soft-hard-soft electron energy distribution and/or low-high-low low-energy cutoff of the electron distribution.

Takakura et al. (1993) reported similar source motions seen with Yohkoh/HXT. In four events they found the hard X-ray source to appear at the top of the flare loop, then to "spreads" along the loop toward the footpoints. After the hard X-ray peak, the source became a single source at the looptop. Because of the limited energy coverage, this motion could only be seen above 14 keV. The speed of the source "expansion" (∼104 km/s) was higher than what RHESSI shows. Without checking the energy distribution of the moving sources, Takakura et al. (1993) suggested that the motion was caused by electron plasma waves generated in the process of heat conduction. However, it is difficult to explain the energy distribution seen by RHESSI with such a thermal interpretation. Furthermore, such source motions may also have been seen with *Hinotori* (Nitta et al., 1990). In one of the two "short but intenss" flares these authors describe, which would be"early impulsive flare" based on our definition, the *Hinotori* 30-60 keV images showed one coronal source apparently split into two separate loop footpoint sources (Figure 6 of Nitta et al., 1990).

Clearly, the "early impulsive flares" offer us a unique opportunity to search for new signatures for particle acceleration and transport in solar flares.

7. Theory

7.1. Footpoint-to-looptop ratio

[This subject is closely allied to the coronal thick-target modeling, so perhaps we don't need it. However there is a some theoretical development not yet covered, and we should get Alec to deal with it ; see Melrose and Brown, 1976, MacKinnon, 1988, Fletcher and Martens, 1998, Petrosian et al., 2002, Tomczak and Ciborski, 2007 – HH]

7.2. Collapsing traps

Hugh and Astrid will draft this, hopefully with help from others, e.g. Alec – HH

[It seems to me that there are three items to cover here: betatron acceleration, Fermi acceleration, and inductive electrodynamical effects. I am not sure there is any literature at all on the last item! – HH]

[It would be particularly interesting to hear how the collapsing-trip scenario ties in with the distributed electric fields discussed by Drake et al. (2006) and Onofri et al. (2006) – HH]

7.3. Particle acceleration mechanisms

[In a sense, the most important part of the picture! Presumably some combination of Peter, Loukas, Lyndsay, and Alec will work on this – HH]

8. Conclusions

[A 3D time/space/spectrum spectrogram representation of July 23, illustrating when and how the different components appear); see the placeholder in Figure 15 for a bad beginning]

Acknowledgements

NASA NAG5-12878 (HSH, SK)

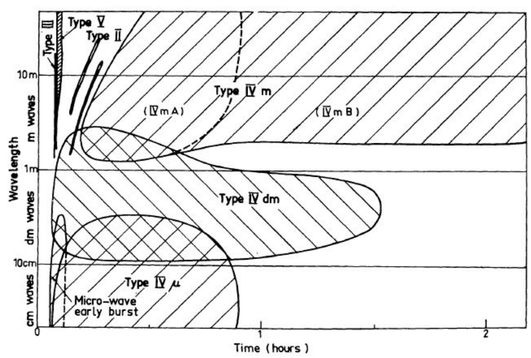

Figure 15. Place holder for a summary sketch showing when and where different kinds of coronal hard X-ray emissions occur, and what their spectral distributions are (this figure is from Wild et al., 1963. I am sure that we can do better, and at the same time avoid getting hung up in nomenclature - HH).

9. Appendix A: Emission mechanisms revisited

[Team member Alec is working on this – HH]

Stein & Ney? Shklovsky book? Korchak, 1967

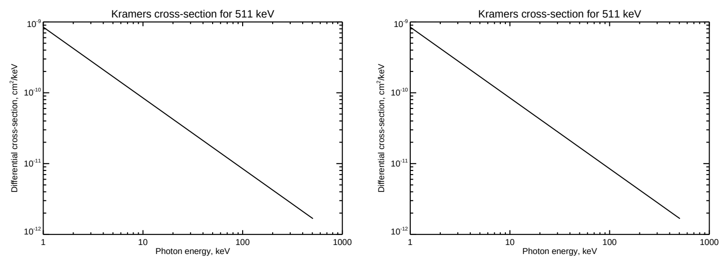

Figure 16. Left, the Kramers cross-section, differential in photon energy for 511 keV electrons. Right, the surface brightness of the Newkirk coronal density model, as a function of projected height (see text).

10. Appendix B: Aids to interpretation

[If we are energetic enough, this section should contain a lot of information useful for the interpretation of hard X-ray sources in the corona. This is a list of some of the items we might think to include. In my imagination I also see us actually using some of these plots, or even the software that made them, to help analyze individual events at ISSI - HH]

Bremsstrahlung cross-section: The Kramers cross-section (Figure 16) is a good rough-and-ready way to estimate the coronal non-thermal bremsstrahlung flux. This is $\Sigma = \sigma_0 \bar{Z}^2/\epsilon E$ where $\sigma_0 = 7.9 \times 10^{24}$ cm^2. We take $\bar{Z}^2 = 1.4$.

Coulomb collisional cross-sections

Magnetic models and particle drifts: The PFSS modeling of the solar coronal magnetic field has reached a certain level of maturity and convenience (e.g., Schrijver and Derosa, 2003. For example, meter-wave images of type III radio bursts can correctly be identified with open field lines in such models (Klein, Nitta, work in progress?). We can probably thus begin to think of fitting specific large-scale field geometries to specific coronal hard X-ray events. Figure 17 shows an example for the January 2005 region.

Three-dimensional projections: The coronal surface brightness depends on the geometry of the source, which we take to be a set of loops of unknown angles relative to the line of sight. See Loughhead et al. (1983), Berton and Sakurai (1985), and Nitta (2000), for example, for discussions of this point.

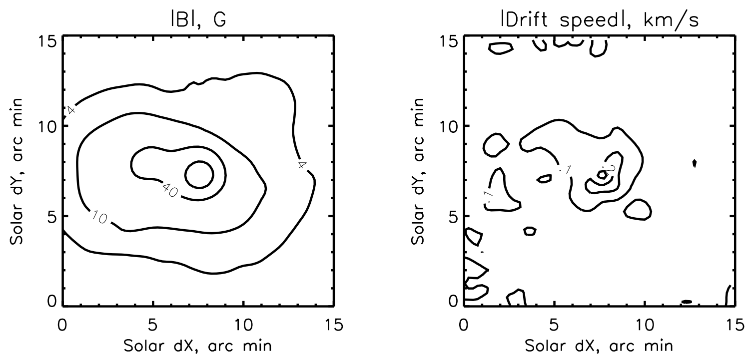

Figure 17. Example of a PFSS magnetic map for the January 2005 active region. Left, contours of B magnitude at 35,000 km altitude for 16 January 2005 (in Gauss); the peak B was about 160G. Right, the magnitude of the adiabatic drift speed for a 511-keV proton in this field (note - this may be wildly wrong but at least illustrates the possibility - HH).

For ease of interpretation Figure 16 (right panel) shows the surface brightness of a model hard X-ray source for the following conditions: Newkirk density model, solid angle 8.5×10^{-8} sr (one arcmin^2), for a monoenergetic (511 keV) nonthermal particle population at a density 1% of the ambient density.

References

Acton, L. W., U. Feldman, M. E. Bruner, G. A. Doschek, T. Hirayama, H. S. Hudson, J. R. Lemen, Y. Ogawara, K. T. Strong, and S. Tsuneta: 1992, 'The morphology of 20 X 10 exp 6 K plasma in large non-impulsive solar flares'. *PASJ* **44**, L71–L75.

Alexander, D. and T. R. Metcalf: 2002, 'Energy dependence of electron trapping in a solar flare'. *Solar Phys* **210**, 323–340.

Antiochos, S. K. and P. A. Sturrock: 1978, 'Evaporative cooling of flare plasma'. *ApJ* **220**, 1137–1143.

Arzner, K. and A. O. Benz: 2005, 'Temporal Correlation of Hard X-Rays and Meter/Decimeter Radio Structures in Solar Flares'. *Solar Phys* **231**, 117–141.

Asai, A., H. Nakajima, M. Shimojo, S. M. White, H. S. Hudson, and R. P. Lin: 2006, 'Preflare Nonthermal Emission Observed in Microwaves and Hard X-Rays'. *PASJ* **58**, L1–L5.

Asai, A., T. Yokoyama, M. Shimojo, and K. Shibata: 2004, 'Downflow Motions Associated with Impulsive Nonthermal Emissions Observed in the 2002 July 23 Solar Flare'. *ApJL* **605**, L77–L80.

Aschwanden, M. J., A. O. Benz, B. R. Dennis, and R. A. Schwartz: 1995, 'Solar Electron Beams Detected in Hard X-Rays and Radio Waves'. *ApJ* **455**, 347–+.

Aschwanden, M. J., L. Fletcher, T. Sakao, T. Kosugi, and H. Hudson: 1999, 'Deconvolution of Directly Precipitating and Trap-precipitating Electrons in Solar Flare Hard X-Rays. III. Yohkoh Hard X-Ray Telescope Data Analysis'. *ApJ* **517**, 977–989.

Aurass, H., K.-L. Klein, and P. C. H. Martens: 1994, 'First detection of correlated electron beams and plasma jets in radio and soft x-ray data'. *Solar Phys* **155**, 203–206.

Bai, T. and P. A. Sturrock: 1989, 'Classification of solar flares'. *ARAA* **27**, 421–467.

Battaglia, M. and A. O. Benz: 2006, 'Relations between concurrent hard X-ray sources in solar flares'. *A&A* **456**, 751–760.

Battaglia, M. and A. O. Benz: 2007a, 'Exploring the connection between coronal and footpoint sources in a thin-thick target solar flare model'. *ArXiv Astrophysics e-prints*.

Battaglia, M. and A. O. Benz: 2007b, 'Exploring the connection between coronal and footpoint sources in a thin-thick target solar flare model'. *ArXiv Astrophysics e-prints*.

Benz, A. O., P. C. Grigis, A. Csillaghy, and P. Saint-Hilaire: 2005, 'Survey on Solar X-ray Flares and Associated Coherent Radio Emissions'. *Solar Phys* **226**, 121–142.

Berton, R. and T. Sakurai: 1985, 'Stereoscopic determination of the three-dimensional geometry of coronal magnetic loops'. *Solar Phys* **96**, 93–111.

Bone, L., J. C. Brown, L. Fletcher, A. Veronig, and S. White: 2007, 'Birth and evolution of a dense coronal loop in a complex flare region'. *A&A* **446**, 339–346.

Brown, J. C.: 1971a, 'The Deduction of Energy Spectra of Non-Thermal Electrons in Flares from the Observed Dynamic Spectra of Hard X-Ray Bursts'. *Solar Phys* **18**, 489–+.

Brown, J. C.: 1971b, 'The Deduction of Energy Spectra of Non-Thermal Electrons in Flares from the Observed Dynamic Spectra of Hard X-Ray Bursts'. *Solar Phys* **18**, 489–+.

Brown, J. C.: 1973, 'The Temperature Structure of Chromospheric Flares Heated by Non-Thermal Electrons'. *Solar Phys* **31**, 143–+.

Brown, J. C., M. J. Aschwanden, and E. P. Kontar: 2002, 'Chromospheric Height and Density Measurements in a Solar Flare Observed with RHESSI I. Theory'. *Solar Phys* **210**, 373–381.

Cliver, E. W., B. R. Dennis, A. L. Kiplinger, S. R. Kane, D. F. Neidig, N. R. Sheeley, and M. J. Koomen: 1986, 'Solar gradual hard X-ray bursts and associated phenomena'. *ApJ* **305**, 920–935.

Daibog, E. I., E. A. Devicheva, V. G. Kurt, I. I. Logachev, A. V. Nogteva, V. G. Stopovskii, S. V. Golenetskii, I. A. Gurian, and A. Varga: 1981, 'Energy spectra of high energy electrons and hard X-rays as observed onboard the space probe Venera 11 during the solar flare event of April 13 1979'. *Advances in Space Research* **1**, 73–76.

Drake, J. F., M. Swisdak, H. Che, and M. A. Shay: 2006, 'Electron acceleration from contracting magnetic islands during reconnection'. *Nature* **443**, 553–556.

Fárník, F., H. S. Hudson, M. Karlický, and T. Kosugi: 2003, 'X-ray and radio observations of the activation stages of an X-class solar flare'. *A&A* **399**, 1159–1166.

Fletcher, L. and P. C. H. Martens: 1998, 'A Model for Hard X-Ray Emission from the Top of Flaring Loops'. *ApJ* **505**, 418–431.

Frost, K. J. and B. R. Dennis: 1971, 'Evidence from Hard X-Rays for Two-Stage Particle Acceleration in a Solar Flare'. *ApJ* **165**, 655–+.

Garcia, H. A.: 1994, 'Temperature and emission measure from GOES soft X-ray measurements'. *Solar Phys* **154**, 275–308.

Goff, C. P., L. van Driel-Gesztelyi, L. K. Harra, S. A. Matthews, and C. H. Mandrini: 2005a, 'A slow coronal mass ejection with rising X-ray source'. *A&A* **434**, 761–771.

Goff, C. P., L. van Driel-Gesztelyi, L. K. Harra, S. A. Matthews, and C. H. Mandrini: 2005b, 'A slow coronal mass ejection with rising X-ray source'. *A&A* **434**, 761–771.

Grigis, P. C. and A. O. Benz: 2004, 'The spectral evolution of impulsive solar X-ray flares'. *A&A* **426**, 1093–1101.

Hoyng, P., H. F. van Beek, and J. C. Brown: 1976, 'High time resolution analysis of solar hard X-ray flares observed on board the ESRO TD-1A satellite'. *Solar Phys* **48**, 197–254.

Hudson, H. and J. Ryan: 1995, 'High-Energy Particles In Solar Flares'. *ARAA* **33**, 239–282.

Hudson, H. S.: 1972, 'Thick-Target Processes and White-Light Flares'. *Solar Phys* **24**, 414–+.

Hudson, H. S.: 1978, 'A purely coronal hard X-ray event'. *ApJ* **224**, 235–240.

Hudson, H. S. and F. Fárník: 2002, 'Spectral variations of flare hard X-rays'. In: A. Wilson (ed.): *ESA SP-506: Solar Variability: From Core to Outer Frontiers*. pp. 261–264.

Hudson, H. S., T. Kosugi, N. V. Nitta, and M. Shimojo: 2001, 'Hard X-Radiation from a Fast Coronal Ejection'. *ApJL* **561**, L211–L214.

Hudson, H. S., R. P. Lin, and R. T. Stewart: 1982, 'Second-stage acceleration in a limb-occulted flare'. *Solar Phys* **75**, 245–261.

Jiang, Y. W., S. Liu, W. Liu, and V. Petrosian: 2006, 'Evolution of the Loop-Top Source of Solar Flares: Heating and Cooling Processes'. *ApJ* **638**, 1140–1153.

Kahler, S.: 1976, 'Determination of the energy or pressure of a solar X-ray structure using X-ray filtergrams from a single filter'. *Solar Phys* **48**, 255–259.

Kane, S. R.: 1972, 'Evidence for a Common Origin of the Electrons Responsible for the Impulsive X-Ray and Type III Radio Bursts'. *Solar Phys* **27**, 174–+.

Kane, S. R., K. A. Anderson, W. D. Evans, R. W. Klebesadel, and J. Laros: 1979, 'Observation of an impulsive solar X-ray burst from a coronal source'. *ApJL* **233**, L151–L155.

Kane, S. R., R. W. Kreplin, M.-J. Martres, M. Pick, and I. Soru-Escaut: 1974, 'Acceleration of electrons in absence of detectable optical flares deduced from type III radio bursts, H alpha activity and soft X-ray emission'. *Solar Phys* **38**, 483–497.

Kiplinger, A. L.: 1995, 'Comparative Studies of Hard X-Ray Spectral Evolution in Solar Flares with High-Energy Proton Events Observed at Earth'. *ApJ* **453**, 973–+.

Korchak, A. A.: 1967, 'Possible Mechanisms for Generating Hard X Rays in Solar Flares.'. *Soviet Astronomy* **11**, 258–+.

Kosugi, T., T. Sakao, S. Masuda, H. Hara, T. Shimizu, and H. S. Hudson: 1994, 'Hard and Soft X-ray Observations of a Super-Hot Thermal Flare of 6 February, 1992'. In: *Proceedings of Kofu Symposium*. pp. 127–129.

Kosugi, T., T. Sakao, S. Masuda, K. Makishima, M. Inda, T. Murakami, Y. Ogawara, K. Yaji, and K. Matsushita: 1992, 'The Hard X-ray Telescope (HXT) onboard YOHKOH - Its performance and some initial results'. *PASJ* **44**, L45–L49.

Krucker, S. and R. Lin: 2007.

Lin, R. P.: 1970, 'The Emission and Propagation of ˜ 40 keV Solar Flare Electrons. II: The Electron Emission Structure of Large Active Regions'. *Solar Phys* **15**, 453–+.

Lin, R. P., S. Krucker, G. D. Holman, L. Sui, G. J. Hurford, and R. A. Schwartz: 2003a, 'RHESSI Discovery of a Coronal Non-Thermal Hard X-Ray Source in the 23 July 2002 Gamma-Ray Line Flare'. In: *International Cosmic Ray Conference*, Vol. 6 of *International Cosmic Ray Conference*. pp. 3207–+.

Lin, R. P., S. Krucker, G. J. Hurford, D. M. Smith, H. S. Hudson, G. D. Holman, R. A. Schwartz, B. R. Dennis, G. H. Share, R. J. Murphy, A. G. Emslie, C. Johns-Krull, and N. Vilmer: 2003b, 'RHESSI Observations of Particle Acceleration and Energy Release in an Intense Solar Gamma-Ray Line Flare'. *ApJL* **595**, L69–L76.

Lin, R. P., R. A. Schwartz, R. M. Pelling, and K. C. Hurley: 1981, 'A new component of hard X-rays in solar flares'. *ApJL* **251**, L109–L114.

Lin, R. P. *et al.*.: 2002, 'High spectral resolution measurements of a solar flare hard X-ray burst'. *Solar Phys.* **210**.

Loughhead, R. E., J.-L. Wang, and G. Blows: 1983, 'High-resolution photography of the solar chromosphere. XVII Geometry of H-alpha flare loops observed on the disk'. *ApJ* **274**, 883–899.

MacKinnon, A. L.: 1988, 'Coulomb collisional precipitation of fast electrons in solar flares'. *A&A* **194**, 279–287.

Masuda, S., T. Kosugi, H. Hara, S. Tsuneta, and Y. Ogawara: 1994, 'A Loop-Top Hard X-Ray Source in a Compact Solar Flare as Evidence for Magnetic Reconnection'. *Nature* **371**, 495.

Melrose, D. B. and J. C. Brown: 1976, 'Precipitation in trap models for solar hard X-ray bursts'. *MNRAS* **176**, 15–30.

Metcalf, T. R. and D. Alexander: 1999, 'Coronal Trapping of Energetic Flare Particles:Yohkoh/HXT Observations'. *ApJ* **522**, 1108–1116.

Neupert, W. M.: 1968, 'Comparison of Solar X-Ray Line Emission with Microwave Emission during Flares'. *ApJL* **153**, L59+.

Nitta, N.: 2000, 'Flare Loop Geometry'. In: R. Ramaty and N. Mandzhavidze (eds.): *ASP Conf. Ser. 206: High Energy Solar Physics Workshop - Anticipating Hessi*. pp. 258–+.

Nitta, N., B. R. Dennis, and A. L. Kiplinger: 1990, 'X-ray observations of two short but intense solar flares'. *ApJ* **353**, 313–322.

Onofri, M., H. Isliker, and L. Vlahos: 2006, 'Stochastic Acceleration in Turbulent Electric Fields Generated by 3D Reconnection'. *Physical Review Letters* **96**(15), 151102–+.

Palmer, I. D. and S. F. Smerd: 1972, 'Evidence for a Two-Component Injection of Cosmic Rays from the Solar Flare of 1969, March 30'. *Solar Phys* **26**, 460–+.

Pan, L.-D., R. P. Lin, and S. R. Kane: 1984, 'Comparison of solar flare X-ray producing and escaping electrons from about 2 to 100 keV'. *Solar Phys* **91**, 345–357.

Parks, G. K. and J. R. Winckler: 1969, 'Sixteen-Second Periodic Pulsations Observed in the Correlated Microwave and Energetic X-Ray Emission from a Solar Flare'. *ApJ* **155**, L117–+.

Petrosian, V., T. Q. Donaghy, and J. M. McTiernan: 2002, 'Loop Top Hard X-Ray Emission in Solar Flares: Images and Statistics'. *ApJ* **569**, 459–473.

Prince, T. A., G. J. Hurford, H. S. Hudson, and C. J. Crannell: 1988, 'Gamma-ray and hard X-ray imaging of solar flares'. *Solar Phys* **118**, 269–290.

Qiu, J., J. Lee, and D. E. Gary: 2004, 'Impulsive and Gradual Nonthermal Emissions in an X-Class Flare'. *ApJ* **603**, 335–347.

Ramsey, B. D., C. D. Alexander, J. A. Apple, R. A. Austin, C. M. Benson, K. L. Dietz, R. F. Elsner, D. E. Engelhaupt, J. J. Kolodziejczak, S. L. O'Dell, C. O. Speegle, D. A. Swartz, M. C. Weisskopf, and G. Zirnstein: 2000, 'HERO: high-energy replicated optics for a hard-x-ray balloon payload'. In: R. B. Hoover and A. B. Walker (eds.): *Proc. SPIE Vol. 4138, p. 147-153, X-Ray Optics, Instruments, and Missions IV, Richard B. Hoover; Arthur B. Walker; Eds.* pp. 147–153.

Raulin, J. P., M. R. Kundu, N. Nitta, and A. Raoult: 1996, 'Radio Continuum and Type III Bursts Associated with Coronal X-Ray Structures'. *ApJ* **472**, 874–+.

Sakao, T.: 1994, 'Characteristics of solar flare hard X-ray sources as revealed with the Hard X-ray Telescope aboard the Yohkoh satellite'. Ph.D. thesis, (University of Tokyo), (1994).

Schrijver, C. J. and M. L. Derosa: 2003, 'Photospheric and heliospheric magnetic fields'. *Solar Phys* **212**, 165–200.

Stewart, R. T.: 1978, 'Relationship between type III-V radio and hard X-ray bursts'. *Solar Phys* **58**, 121–126.

Strong, K. T., A. O. Benz, B. R. Dennis, A. I. Poland, J. W. Leibacher, R. Mewe, J. Schrijver, G. Simnett, J. B. Smith, Jr., and J. Sylwester: 1984, 'A multiwavelength study of a double impulsive flare'. *Solar Phys* **91**, 325–344.

Sui, L., G. D. Holman, and B. R. Dennis: 2004, 'Evidence for Magnetic Reconnection in Three Homologous Solar Flares Observed by RHESSI'. *ApJ* **612**, 546–556.

Sui, L., G. D. Holman, and B. R. Dennis: 2006, 'Motion of 3-6 keV Nonthermal Sources along the Legs of a Flare Loop'. *ApJL* **645**, L157–L160.

Takakura, T., M. Inda, K. Makishima, T. Kosugi, T. Sakao, S. Masuda, T. Sakurai, and Y. Ogawara: 1993, 'Time variation of the hard X-ray image during the early phase of solar impulsive bursts'. *PASJ* **45**, 737–753.

Tomczak, M.: 2001, 'The analysis of hard X-ray radiation of flares with occulted footpoints'. *A&A* **366**, 294–305.

Tomczak, M. and T. Ciborski: 2007, 'Footpoint versus loop-top hard X-ray emission sources in solar flares'. *A&A* **461**, 315–323.

Veronig, A. M. and J. C. Brown: 2004, 'A Coronal Thick-Target Interpretation of Two Hard X-Ray Loop Events'. *ApJL* **603**, L117–L120.

Veronig, A. M., J. C. Brown, and L. Bone: 2005, 'Evidence for a solar coronal thick-target hard X-ray source observed by RHESSI'. *Advances in Space Research* **35**, 1683–1689.

Warren, H. P., J. A. Bookbinder, T. G. Forbes, L. Golub, H. S. Hudson, K. Reeves, and A. Warshall: 1999, 'TRACE and Yohkoh Observations of High-Temperature Plasma in a Two-Ribbon Limb Flare'. *ApJL* **527**, L121–L124.

Wheatland, M. S. and D. B. Melrose: 1995a, 'Interpreting YOHKOH hard and soft X-ray flare observations'. *Solar Phys* **158**, 283–299.

Wheatland, M. S. and D. B. Melrose: 1995b, 'Interpreting YOHKOH hard and soft X-ray flare observations'. *Solar Phys* **158**, 283–299.

Wild, J. P., S. F. Smerd, and A. A. Weiss: 1963, 'Solar Bursts'. *ARAA* **1**, 291–+.

Smerd and Weiss, 1971 (March 30 event)

Kontar and Krucker, in preparation